Original Article

3D-QSAR, Molecular Docking, Molecular Dynamics Simulations and Structural Studies of Some Selected Inhibitors of the Glycoprotein (GPC) of Lassa Virus

Emmanuel Israel Edache[a, b, *] | Hadiza Adamu Dawi[a] | Fabian Audu Ugbe[b]

[a]*Department of Pure and Applied Chemistry, University of Maiduguri, Borno State, Nigeria*
[b]*Department of Chemistry, Ahmadu Bello University, P.M.B. 1044, Zaria, Nigeria*

Use your device to scan and read the article online

Citation E.I. Edache, H.A. Dawi, F.A. Ugbe. **3D-QSAR, Molecular Docking, Molecular Dynamics Simulations and Structural Studies of Some Selected Inhibitors of the Glycoprotein (GPC) of Lassa Virus.** *J. Appl. Organomet. Chem.*, **2023**, *3*(3), 224-244.

https://doi.org/10.48309/JAOC.2023.410946.1103

Article info:
Received: 01 August 2023
Accepted: 27 August 2023
Available Online: 31 August 2023
ID: JAOC -2308-1103
Checked for Plagiarism: Yes
Language Editor checked: Yes

Keywords:
Lassa arenavirus, CoMFA-FFD, CoMFA-UVEPLS, Molecular docking, MD simulations

ABSTRACT

3D-QSAR, comparative molecular field analysis- smart region description (SRD) and fractional factorial design (FFD) (CoMFA-FFD), and comparative molecular field analysis-uninformative variable elimination-partial least square (CoMFA-UVEPLS) were conducted on 44 compounds. CoMFA-FFD and CoMFA-UVEPLS models give dependable complementary and prescient capacities; however, the CoMFA-FFD model did was to a little degree or degree better than CoMFA-UVEPLS. From the contour maps generated from the CoMFA-FFD and CoMFA-UVEPLS models, more important features were identified to boast the chemical structures that were responsible for inhibitors of the glycoprotein (GPC) of Lassa (LASV) Arenavirus. Secondly, docking was performed between the compounds and protein to predict their binding affinity. Based on the docking simulation approach, two compounds have chosen for further evaluation. The MD simulation approach was used to confirm the stability of the selected drug candidate to the target protein, which confirmed the stability of the selected lead drugs. Docking and MD simulations present comparative associations between the protein and the ligands. The MD simulations further described hydrogen bond, steric, and hydrophobic interactions on the ligand. The standard free binding energy calculation revealed that the two selected drug candidates have a significant binding affinity for GPC of LASV. The discussion points out positions on the ligands and their suggestions on protein interactions. The computational methodology utilized in this paper gives solid insights for an additional plan of molecules for inhibitors of the glycoprotein (GPC) of Lassa infection (LASV) Arenavirus.

Introduction

The re-emergence and spread of infectious diseases pose a growing public health concern across sub-Saharan Africa [1]. Lassa fever (LF) is becoming more and more alarming in developing countries like Africa due to its high morbidity and mortality [2]. Lassa virus (LSV) is the sole etiologic agent of severe hemorrhagic fever, which is characterized by fever, abdominal pain, sore throat, chest pain, cough, muscular pain, vomiting, and nausea [3]. Relentless fever might check the beginning of

*Corresponding Authors: Emmanuel Israel Edache (edacheson2004@gmail.com)

extreme cases with slender draining from numerous organs and different examples of organ-instigated disappointment [4]. Neurological sequelae, like aseptic meningitis and encephalopathy, may happen in survivors, and hearing misfortune among certain patients [5]. Lassa infection is sent as a zoonotic sickness by ingestion of food and inward breath of sprayers debased with contaminated pee or dung of tainted rodent species (Mastomys natalensis), which fill in as a repository for the LASV [6]. Furthermore, transmission from one human to another is through direct contact with the blood, pee, defecation, or other substantial emissions of a contaminated individual [7]. The disease is endemic in West Africa; recent outbreaks in Nigeria in the wake of the coronavirus pandemic were fatal, larger, and more geographically diverse than usual [8]. The treatment and management of LASV is a plaque by so many factors, crucially, the absence of commercially available LASV diagnostic test kits, which hampers early detection and prompt interventions using existing chemotherapeutic agents [9]. Unfortunately, there are limited chemotherapeutic agents such as the anti-viral drug ribavirin which is most effective in early treatment is a plaque to poor efficacy, cost, and adverse side effects, while the emergence of drug-resistant strains has compromised the efficacy of most antiviral agents [10]; vaccine which is the ideal option is still far from reality [11]. As the world continues to battle the scourge of infectious diseases it is imperative to find a cost-effective and safe antiviral drug against the Lassa fever virus. The glycoprotein (GPC), the only antigen expressed on the viral surface, is the primary target for antibody-mediated neutralization [12].

One approach to this challenge is the use of computational techniques to efficiently identify new drug candidates and targets that are critical to the LASV survival. The LASV nucleoprotein (NP) is an attractive drug target protein with distinctive N- and C- terminal domains linked by a flexible linker [13]. The Lassa virus nucleoprotein (NP) is a multifunctional protein that is essential for many processes in the viral life cycle. These processes include viral replication, transcription, RNA encapsidation, mobilization of ribonucleoprotein complexes to viral budding sites, and inhibition of the host cell's interferon response [14].

For more than three decades, *in silico* drug design has aided pharmaceutical research [15,16]. Two major drug design methodologies are structural-based and ligand-based approaches [17]. The molecular hybridization approach has become one of the most widely used techniques in drug discovery in recent years [18]. *In silico* is a modern approach that has several advantages, including being less expensive, result-situated, limiting creature testing as well as preliminaries and blunders, and being less tedious, to name a few [19]. *In silico* branches like 3D Quantitative Structure-Activity Relationships (3D-QSAR), Docking Simulation, Molecular Dynamics Simulations (MDS), and others have as of late made critical commitments to the improvement of lead and drug candidates [20,21]. A great deal of effort has gone into identifying chemicals that act on enzymes over the last 30 years, and these efforts have resulted in the discovery of several active substances. Edache *et al.* attempted a ligand-based comparative molecular fields analysis (CoMFA-FFD) study for selective HemO inhibitors using computational techniques in the hopes of identifying selective inhibitors [22]. Edache and colleagues used pharmacokinetics and Golden triangle studies of Salicylidene acylhydrazides analogs, as well as docking simulations and molecular dynamics simulations, to screen novel drugs for Chlamydia trachomatis treatment [23]. Alejandro Speck-Planche *et al.* used

homology modeling, linear discriminant analysis, molecular docking, and QSAR studies to develop a betulinic acid analog with a high binding affinity against HIV [24]. Furthermore, Ahmad *et al.* conducted molecular docking, simulation, and MMPBSA studies on Nigella Sativa and Dithymoquinone compounds to identify potential natural antivirals for COVID-19 treatment [25].

This study was therefore carried out to investigate the use of 3D-structure activity, docking simulation, and MDs simulation as tools for drug design, activity prediction, and development, which involve the propagation of a common 3D lattice about a set of molecules and calculation of interaction energies at the framework [26]. The development of a new and effective chemotherapeutic agent would be a key intervention in an attempt to reduce the considerable social and economic impact of LASV and hence the disease eradication.

Experimental

Methods

Source of Dataset

In the Fit_LogAC$_{50}$ and affinity data set of 7,162 tested substances, 239 are active, while 6,168 are inactive. 44 active compounds were selected from the data table provided by National Center for Advancing Translational Sciences were obtained from PubChem [27] with PubChem AID No. 1347082. The chemical structures of all the compounds are presented in **Table 1**, while the PubChem SID, CID number, and Fit_LogAC$_{50}$ are presented in **Table 2**, respectively.

Table 1. List of the ligand's molecules used in this research

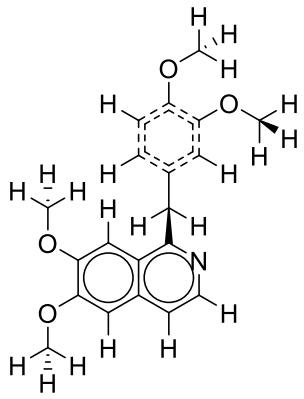

(1)

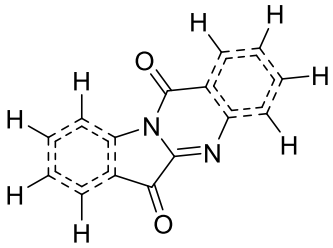

(2)

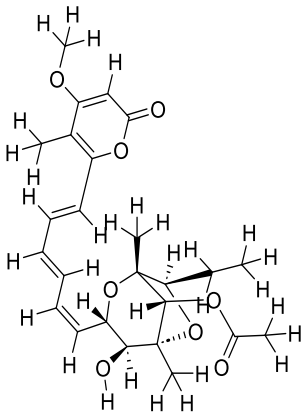

(3)

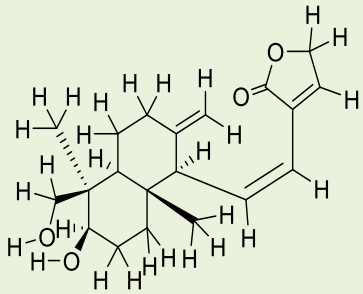

(4)

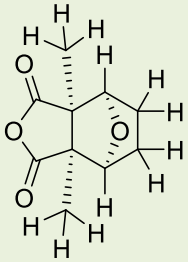

(5)

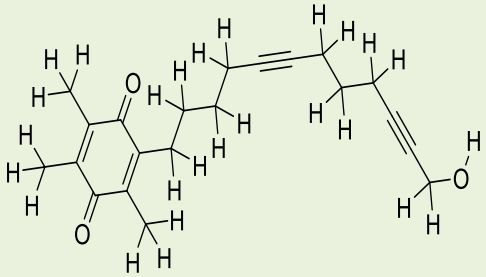

(6)

Table 1. Continued

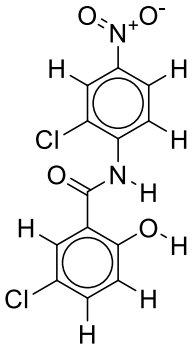 (7)	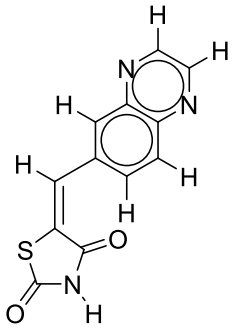 (8)	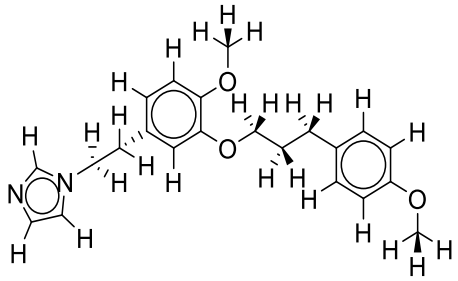 (9)
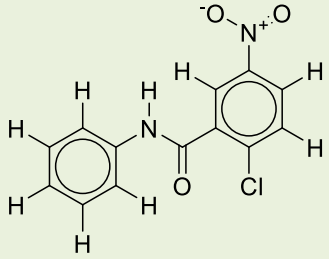 (10)	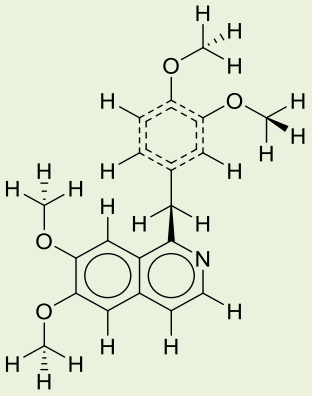 (11)	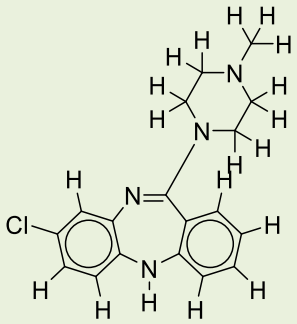 (12)
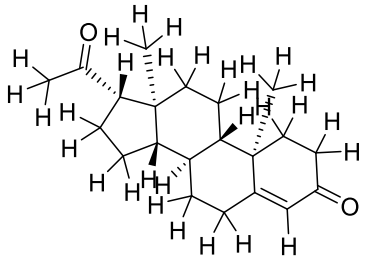 (13)	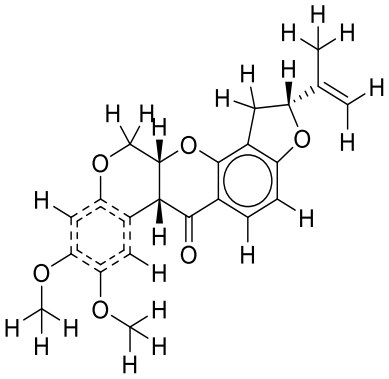 (14)	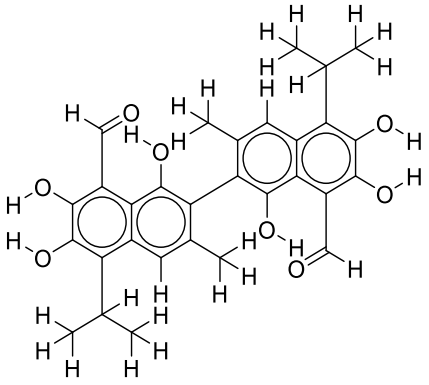 (15)
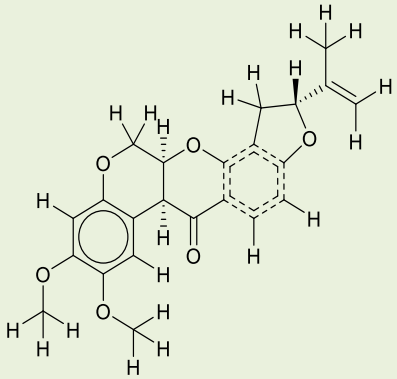 (16)	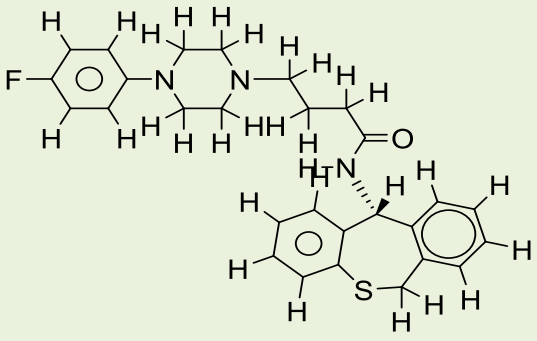 (17)	

Table 1. Continued

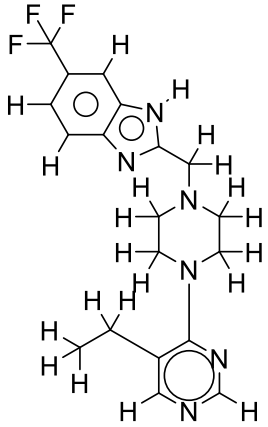

(18)

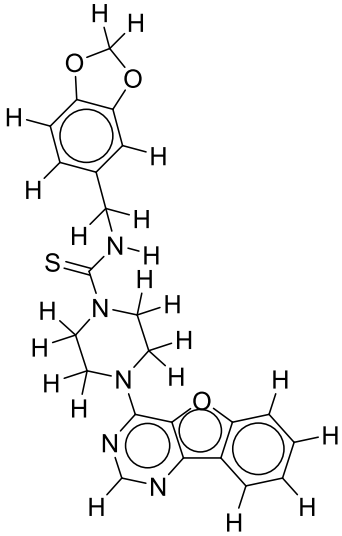

(19)

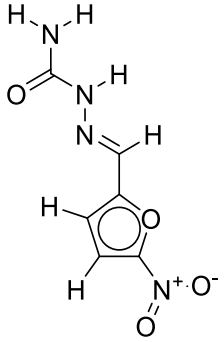

(20)

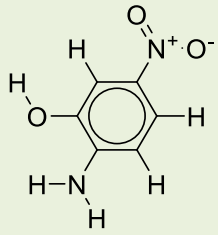

(21)

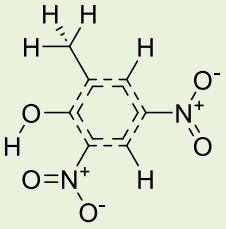

(22)

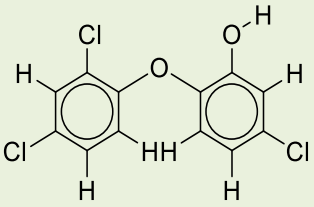

(23)

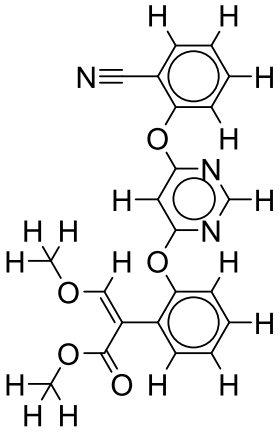

(24)

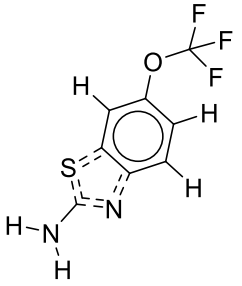

(25)

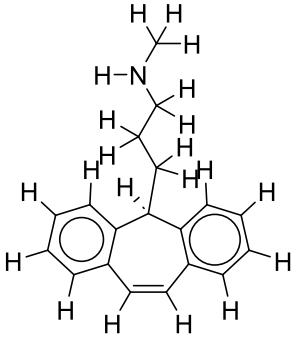

(26)

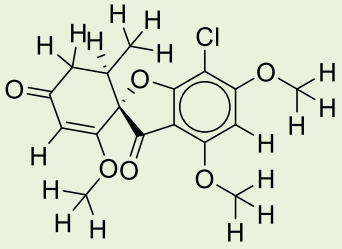

(27)

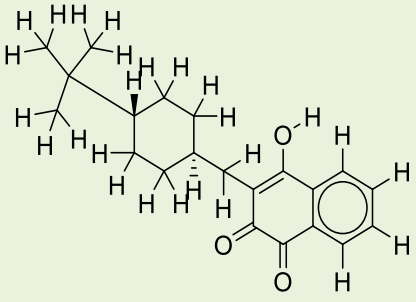

(28)

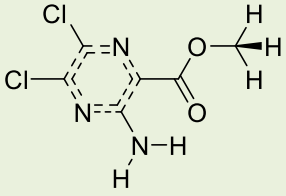

(29)

Table 1. Continued

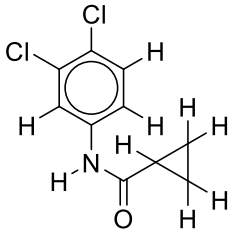

(30)

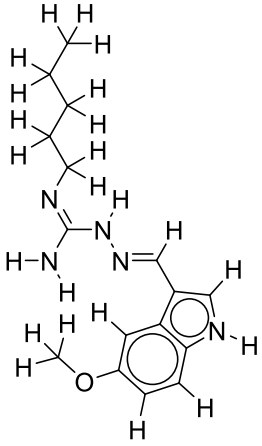

(31)

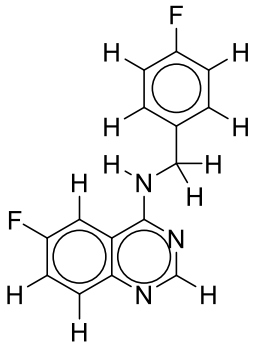

(32)

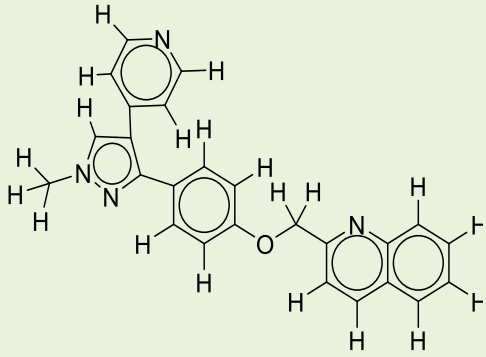

(33)

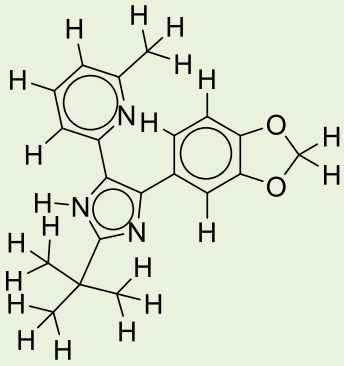

(34)

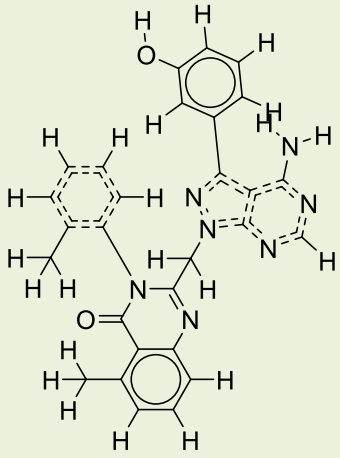

(35)

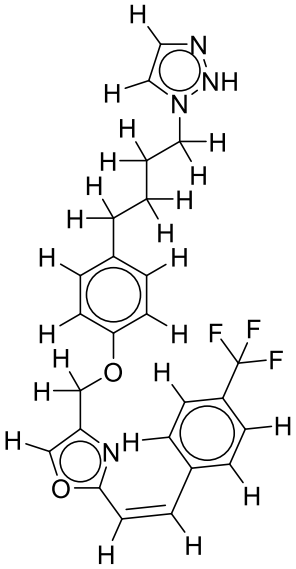

(36)

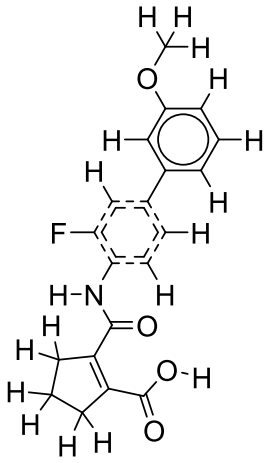

(37)

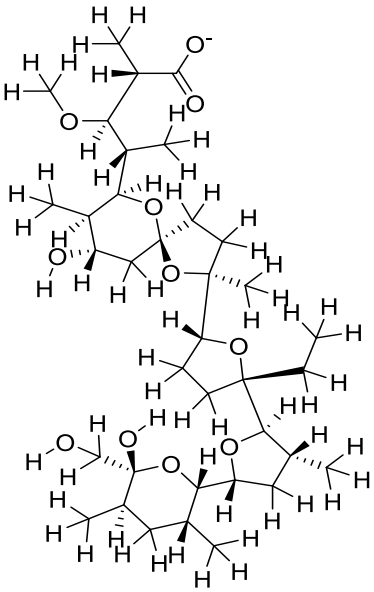

(38)

Table 1. Continued

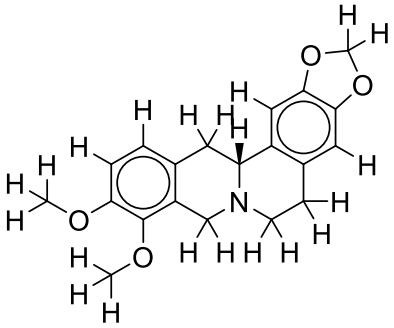

(39)

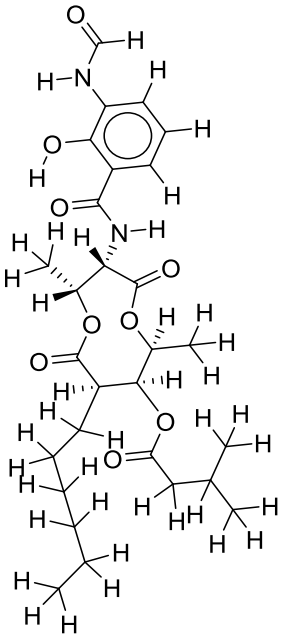

(40)

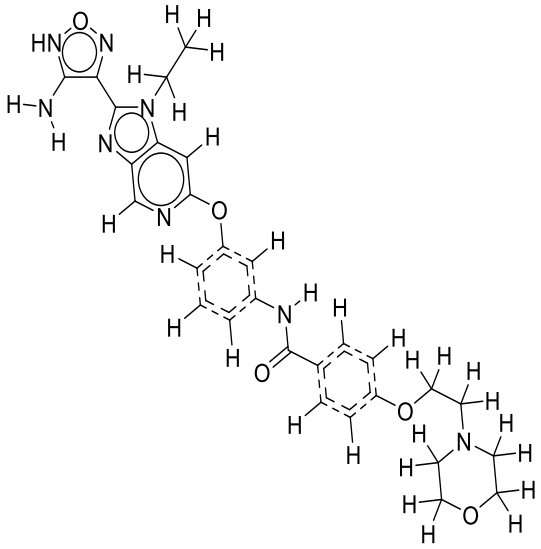

(41)

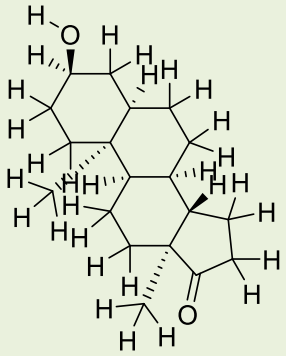

(42)

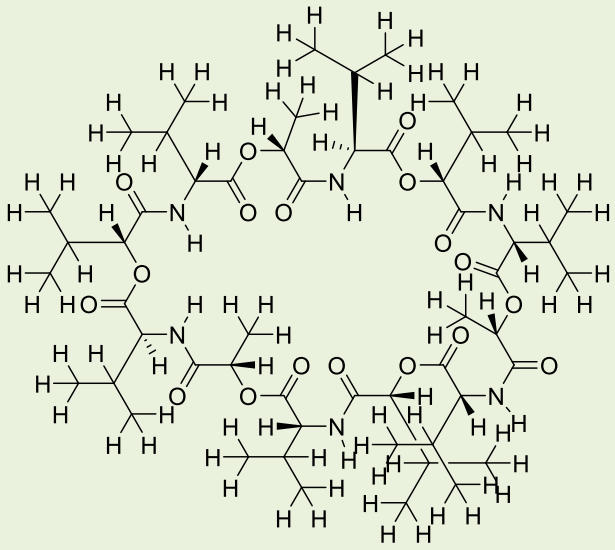

(43)

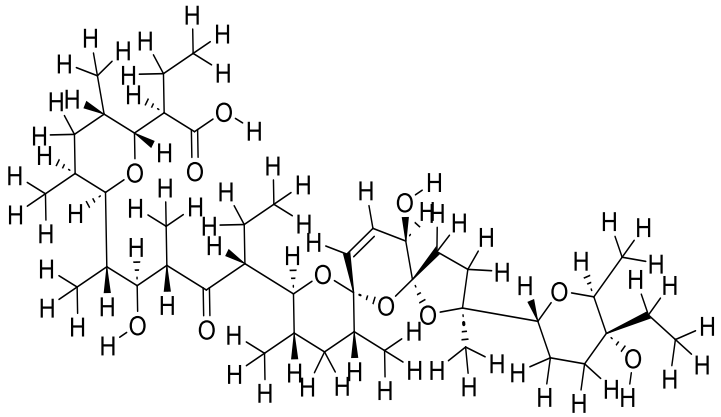

(44)

3D-QSAR Analysis

The compounds were first subjected to energy minimization, then finally optimized by the parameterization method PM6 (a semi-empirical method) using Spartan'14 software [28,29]. The optimized structures were transferred to DTC Lab (v.1.2) software [30], were Kennard-Stone technique was used for data division into training and test set. Where the training set is 30 compounds (70%) and the test set of 14 compounds (30%) was used for the 3D-Quantitative Structure-Activity Relationship model. The exactness of the expectation of 3D-QSAR (CoMFA-FFD and CoMFA-UVEPLS) models and the unwavering quality of the form models rely firmly upon the primary arrangement of the atoms [31]. Open3Dalign software [32] was used for the data set alignment and compound **35** (CID: 24905149) was used as a template for the superimposition. To determine 3D-QSAR models, the CoMFA-FFD and CoMFA-UVEPLS descriptors were utilized as free factors and the Fit_LogAC50 as the reliant variable [33]. PLS strategy was utilized to straightly correspond these CoMFA-FFD and CoMFA-UVEPLS descriptors to the inhibitory activity values. The steric (van der Waals) and electrostatic (coulomb) fields were calculated. The CoMFA-FFD and CoMFA-UVEPLS cutoff values were set to 30 kcal/mol for both steric and electrostatic fields, adjusted particles to a matrix separating (grid spacing) of 2.0 Å in Open3DQSAR [34]. The cross-approval examination was performed using the leave one out (LOO), leave two out (LTO), and leave many out (LMO) method in which one, two, and more compounds, respectively, are eliminated from the data set, and their biological activity is predicted using a model built from the remainder of the data. For subsequent investigation, the cross-validated correlation coefficient (Q2) with the optimum number of components and the lowest standard error of prediction was used.

Molecular Docking

Docking simulations and molecular dynamic simulations helped to understand the ligand-binding mechanisms [35]. Discovery Studio 2020 Client was used to remove the water molecules and all other heteroatoms from the protein crystal structure that was retrieved from protein data bank (PDB). The receptor (PDB id: 5VK2) was assigned Kollman partial charges [36], and then the nonpolar hydrogens of the receptor were added using AutoDock Tools. During the docking computations, the receptor was maintained stiff and all ligand torsional bonds were assumed to be free during docking calculations. Autodock Vina [37] was performed using EasyDockVina v2.2 by creating a center (-53.7122 × 59.4839 × -10.6376), size (44.2198176575 × 37.9585438919 × 72.891568222), and exhaustiveness of 8, around the active site residues protein. Accelrys Discovery Studio 2020 Client examined all of the runs to discover the optimal conformation of the ligand with critical residues in the active region of the protein based on the highest number of clusters and the lowest binding affinity [38].

Molecular Dynamic Simulation

Based on the docking results, molecular dynamics simulations were carried out on the docked protein (Pre-glycoprotein polyprotein GP) complex, the TIP3P water model was used to run the MD simulation and the calculations presented here used the force field CHARMM36 (CHARMM-GUI server) and were run using the NAnoscale Molecular Dynamics program (NAMD) program v2.13 [39]. Periodic boundary conditions are used in MD simulations [40]. The system was neutralized with counterions (0.15 M KCl). Two-step constant number of particles, volume, and temperature (NVT) and constant number of particles, pressure, and temperature (NPT) were carried out. Minimization was used to improve the protein-ligand structure. At 10 ns, the temperature of the system was steadily increased from 0 K to 303.15 K. Subsequently, the system was equilibrated at 303.15 K for 20, 000 run (20 ps) with the NVT ensemble. The simulations were performed in an NPT ensemble and periodic boundary conditions were used. VMD v1.9.3 [41] was used to retrieve and analyze the simulation trajectory.

Computed Binding free energy calculation

The MolAlCal [42] is a program that allows you to generate and analyze accurate binding free energy calculations automatically [43-45]. The MolAlCal software was used to calculate the standard free binding energy of the protein-ligand complexes. The relative binding energy calculations for the complex (RL) formed when the ligand (L) binds to the protein receptor (R), whereby contributions from various interactions can represent by equation (**1**-**3**):

$$\Delta G_{Binding} = \Delta G_{RL} - \Delta G_R - \Delta G_L \quad (1)$$

$$\Delta G_{Binding} = \Delta H - T\Delta S = \Delta E_{MM} + \Delta G_{sol} - T\Delta S \quad (2)$$

$$\Delta E_{MM} = \Delta E_{ele} + \Delta E_{vdw} + \Delta E_{int} \quad (3)$$

Where, $\Delta \boldsymbol{E_{MM}}$ is a combination of the changes in the electrostatic energies $\Delta \boldsymbol{E_{ele}}$, Van der Waals energies $\Delta \boldsymbol{E_{vdw}}$, and internal energies $\Delta \boldsymbol{E_{int}}$, $\Delta \boldsymbol{G_{sol}}$ is the sum of the polar and nonpolar solvations (calculated using the solvent-accessible surface area and the generalized Born model, respectively), and TS is determined by the normal mode analysis. For MM/GBSA calculations, a solvent dielectric constant of 78.5 and a surface tension constant of 0.03012 kJ/ mol[2] were utilized.

Results and Discussion

Using the training set of 30 compounds and the test set of 14 compounds, 3D-QSAR (CoMFA-FFD and CoMFA-UVEPLS) were developed for a data set of 44 compounds for inhibitors of Glycoprotein (GPC) of LASV, an Arenavirus. **Table 2** displays predicted and statistical findings. Visualization of the CoMFA-FFD and CoMFA-UVEPLS model as 3D contour maps was performed using the maestro v10.5.014.

Table 2. Experimental activities (Fit_LogAC50) and projected values of QSAR, Docking scores, CoMFA-FFD, and CoMFA-UVEPLS

No.	PUBCHEM_SID	PUBCHEM_CID	Fit_LogAC50	Docking Scores	CoMFA-FFD (FFDSEL) (predict)	CoMFA-FFD (Residues)	CoMFA-UVEPLS (UVPLS) (predict)	CoMFA-UVEPLS (Residues)
1[T]	26747626	6084	-4.8641	-5.6	-4.6306	-0.2335	-4.7225	-0.1416
2	26754607	73549	-5.4141	-6.2	-5.3249	-0.0892	-5.3176	-0.0965
3	26756900	5353422	-6.9641	-6.2	-7.0035	0.0394	-7.1301	0.166
4	26757024	5708351	-4.3641	-6.2	-4.339	-0.0251	-4.3817	0.0176
5	90340670	2545	-5.4141	-5	-5.184	-0.2301	-5.1868	-0.2273
6	90341036	1967	-4.6141	-5.9	-4.5412	-0.0729	-4.5238	-0.0903
7	90341111	4477	-5.6641	-6.3	-5.6425	-0.0216	-5.6436	-0.0205
8	90341202	5289247	-4.5641	-5.6	-4.8131	0.249	-4.7493	0.1852
9	90341210	4564402	-5.4141	-5.5	-5.4076	-0.0065	-5.3888	-0.0253
10	90341221	644213	-4.6141	-5.4	-4.5212	-0.0929	-4.5247	-0.0894
11	90341237	4680	-4.6641	-5.9	-4.6293	-0.0348	-4.7217	0.0576
12[T]	104171134	135398737	-4.6141	-5.9	-5.0908	0.4767	-5.1324	0.5183
13[T]	124881022	5994	-4.7141	-6.5	-5.5296	0.8155	-5.5577	0.8436
14	124881348[o]	5102	-7.0141	-7.6	Out	-	Out	-
15	124882242	3503	-4.6641	-6.8	-4.6278	-0.0363	-4.5733	-0.0908
16	124883112	6758	-6.7141	-6.4	-6.8097	0.0956	-6.8129	0.0988
17	124894552	60810	-7.7641	-7.9	-7.6841	-0.08	-7.7153	-0.0488
18	137275978	51371303	-4.9029	-7	-4.8954	-0.0075	-4.8947	-0.0082
19[T]	137276002	11282283	-5.0529	-8	-5.8129	0.76	-5.6266	0.5737

Table 2. Continued

20[T]	144204548	5447130	-5.2141	-5.5	-4.8571	-0.357	-4.7744	-0.4397
21	144213997	4984721	-4.4029	-5.3	-4.5121	0.1092	-4.5286	0.1257
22	144214029	10800	-4.0529	-5.4	-4.2728	0.2199	-4.3201	0.2672
23	144214040	5564	-4.4029	-5.3	-4.4781	0.0752	-4.4524	0.0495
24	144214048	3034285	-4.5029	-6.4	-4.5932	0.0903	-4.5826	0.0797
25	170464928	5070	-4.6141	-5.3	-4.5498	-0.0643	-4.4978	-0.1163
26[T]	170465077	6603149	-4.6141	-6.1	-4.4976	-0.1165	-4.5205	-0.0936
27	170465739	441140	-4.9141	-5.5	-4.7502	-0.1639	-4.7942	-0.1199
28	170466326	71768	-4.5141	-7.1	-4.4922	-0.0219	-4.4799	-0.0342
29	170466763	73828	-5.7141	-5.6	-5.812	0.0979	-5.756	0.0419
30[o]	170466836	17693	-8.8641	-4.8	Out	-	out	-
31[T]	170466887	135409453	-5.0641	-5.2	-5.1409	0.0768	-5.1358	0.0717
32[T]	174006174	51037431	-4.8141	-6.6	-5.0146	0.2005	-4.9749	0.1608
33[T]	174006264	11581936	-4.6641	-7.4	-5.5827	0.9186	-5.3342	0.6701
34	174006489	9858940	-5.3141	-6.9	-5.3315	0.0174	-5.29	-0.0241
35	174006522	24905149	-4.4141	-8	-4.3974	-0.0167	-4.5019	0.0878
36[T]	174006556	204100	-7.1141	-7.4	-5.1844	-1.9297	-5.2631	-1.851
37	174007069	9820008	-5.0641	-7.3	-5.1622	0.0981	-5.1845	0.1204
38	174007192	73265358	-5.3753	-7.3	-5.2721	-0.1032	-5.3739	-0.0014
39	174007450	73265409	-6.8141	-6.1	-4.9292	-1.8849	-4.8406	-1.9735
40	174007463	14957	-7.2641	-6.7	-7.2856	0.0215	-7.1849	-0.0792
41	385219832	16095342	-5.0641	-7.4	-5.0548	-0.0093	-5.0253	-0.0388
42[T]	385219833	7056470	-4.6075	-6.8	-4.1751	-0.4324	-4.2826	-0.3249
43	385219837	16667711	-5.9141	-6.3	-5.9619	0.0478	-5.9013	-0.0128
44[T]	385219838	65452	-5.8029	-6.9	-5.3904	-0.4125	-5.5004	-0.3025
REFERENCE/ STANDARD DRUGS								
1	Ribavirin	37542		-5.7				
2	Ruxolitinib	25126798		-6.2				
3	Lopinavir	92727		-6.8				
4	Ritonavir_	392622		-6				
5	Azithromycin	447043		-7.4				

[T]Test set, [o]Outliers, [ffdsel]COMFA-FFD, and [uvepls]COMFA-UVEPLS.

Based on the FFD procedure, the CoMFA-FFD model results have good coefficients of determination of $Q^2_{(LOO)}$ of 0.6439, $Q^2_{(LTO)}$ of 0.5567, and $Q^2_{(LMO)}$ of 0.55 of the cross-validation predictions, respectively. The partial least square (PLS) regression gave a non-cross-validated relationship coefficient (R^2) of 0.9876 with an extremely low standard error estimate (SEE) of 0.1006 and an F-test worth of 382.7035. The CoMFA-FFD model utilizing compound **35** as a kind of perspective construction was converted into shape guides (contour maps) of both steric and electrostatic impacts for inhibitors of the Glycoprotein (GPC) of LASV (see **Figures 1** and **2**, separately). The steric contributed 72.21% (**Figure 1**(**A** and **B**)), and electrostatic contribute 27.29% (**Figure 1**(**C** and **D**)), respectively.

The steric field and electrostatic interaction are addressed by red and blue forms in which blue shapes demonstrate districts where the massive gathering would be great while the red forms address areas where the cumbersome (i.e., steric bulky groups) gathering would diminish the activity. As presented in **Figure 1A**, the steric interaction, the red contour map contributes 70.73% indicating less cumbersome gatherings at this position would

increase the effectiveness while in **Figure 1B**, the blue contour map contributes 29.27% which suggests that cumbersome gatherings at that region would increase the effectiveness of the compounds. The electrostatic contour map is shown in **Figure 1**(**C** and **D**), the red region which represents 48.91% of the contour map indicates that the presence of the electron-donating group would increase the bioactivity remarkably. Electron-withdrawing groups (blue contour, **Figure 1D**) would increase the bioactivity.

The CoMFA-UVEPLS model uses compound **41** as a reference structure (**Figure 2A** to **2D**), for inhibitors of the Glycoprotein (GPC) of LASV. The steric contributed 65.51% (**Figure 2A** and **2B**), and electrostatic contribute 34.49% (**Figure 2C** and **2D**), respectively. The partial least square (PLS) regression gave a non-cross-validated correlation coefficient (R^2) of 0.9857 with a very low standard error estimate (SEE) of 0.1083 and an F-test value of 329.7039 were obtained, where the SDEP of 0.6010 and coefficient of determination (leave one out, leave two, and leave many out) are 0.5580, 0.5429, and 0.4683, respectively. The CoMFA-UVEPLS results show that 3D-QSAR models are trustworthy and can reliably estimate binding affinities of novel derivatives. Red contours (78.19 percent) indicate where bulky groups decrease activity, whereas blue contour areas (21.81 percent) indicate where bulky groups increase inhibitory activity in the CoMFA-UVEPLS steric interaction, as illustrated in **Figure 2**(**A** and **B)**, respectively. The red and blue contours in the electrostatic interaction reflect the negative (unfavorable) and positive (favorable) areas, respectively. The red contour map accounts for 46.18 percent of the total, while the blue contour accounts for 53.82 percent. As a result, an electronegative molecular fragment near a blue area would not boost the chemical bioactivity, whereas an electropositive would. The red contour, which is an electronegative fragment, would be beneficial to the compound's bioactivity.

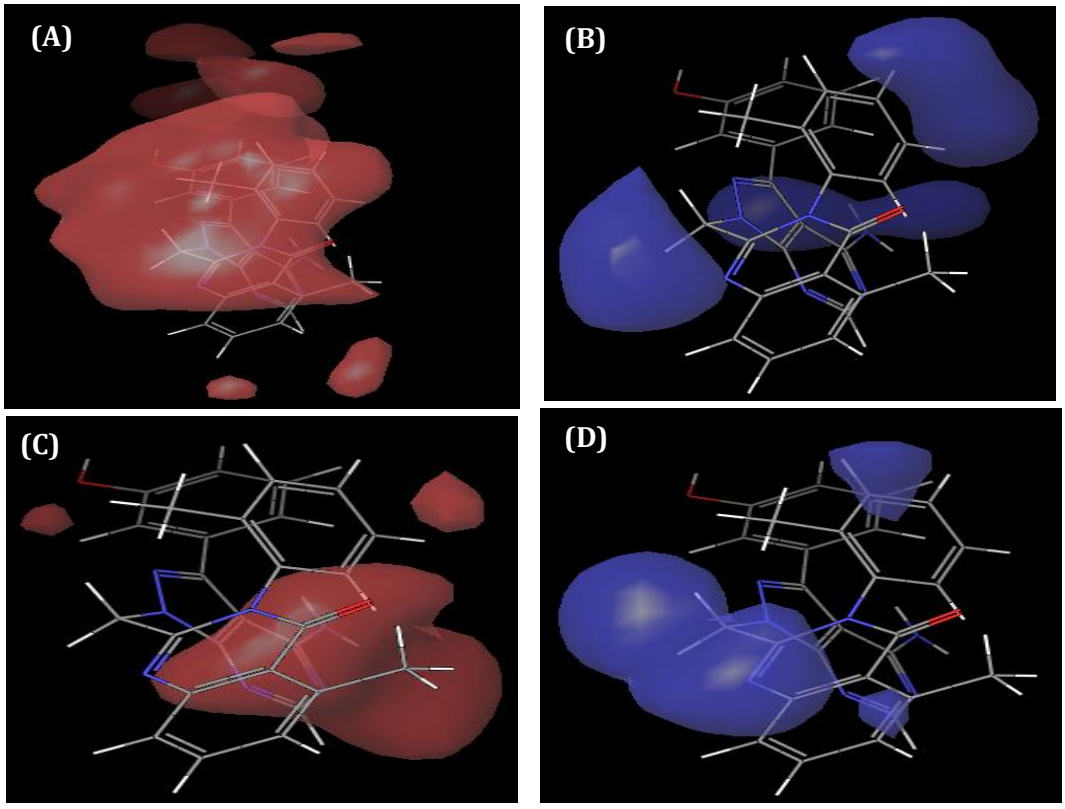

Figure 1. Map of the steric contours red and blue contours illustrate places where bulky groups increase or reduce activity in CoMFA-FFD (A and B). Graph of electrostatic contours red and blue contours illustrate places where electron-donating or electron-withdrawing groups increase potency in CoMFA-FFD (C and D)

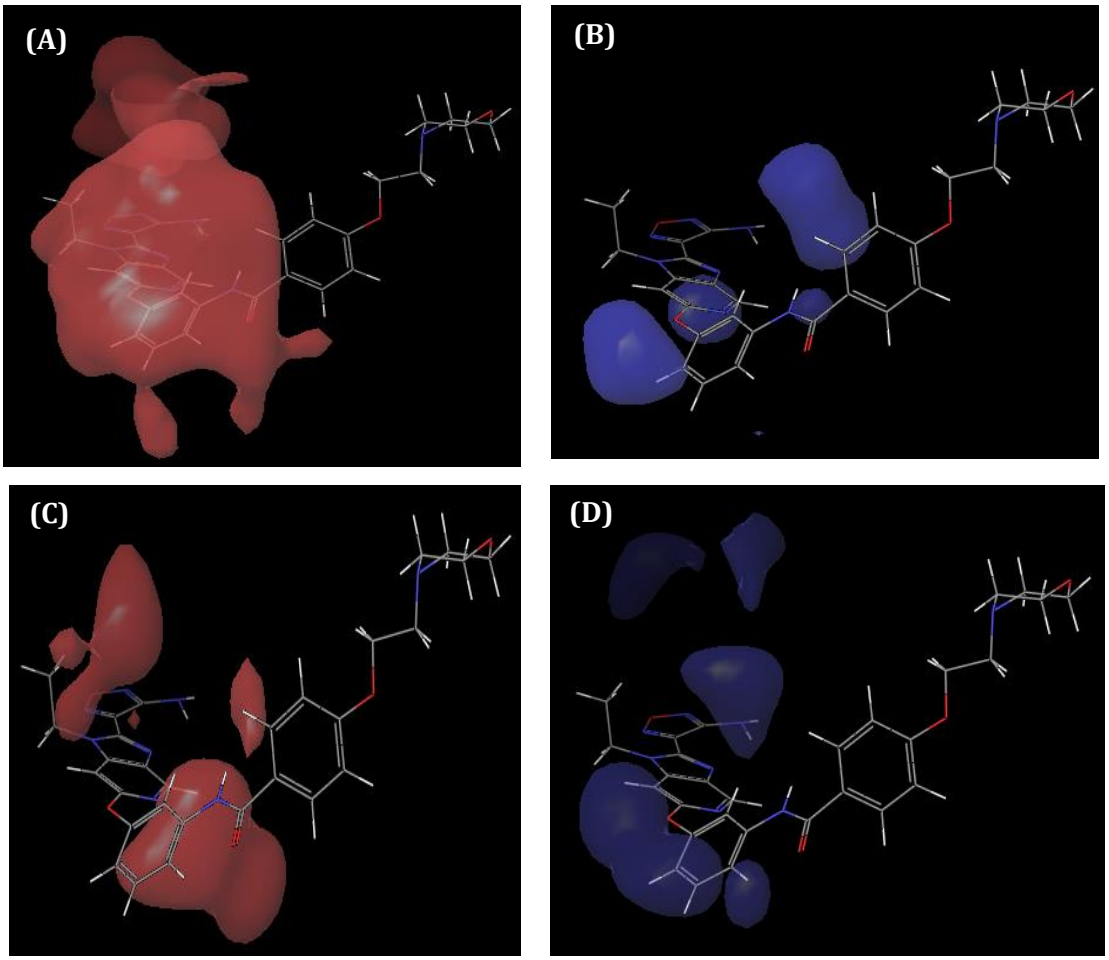

Figure 2. Steric (A and B) CoMFA-UVEPLS contours. Bulky group activity is shown by red outlines where it declines and by blue areas when it increases. (C and D) Electrostatic. Negative groups tend to increase activity in red outlines, whereas positive groups tend to increase activity in blue areas

Docking Results

All the compounds with PUBCHEM_CID code were docked into the limiting site of protein, PDB code: 5VK2 (Pre-glycoprotein polyprotein GP complex), and the limiting partiality scores of the ligand-protein edifices are additionally listed in **Table 2**. Since the docking results are touchy to the scoring capacity. The one with the lowest docking score (compound **19**, -8.00 kcal/mol, and compound **35**, -8.00 kcal/mol) is selected for discussion.

The docking result shows that binding affinity for compound 19 and compound **35** are less than the reference drugs (Ampicillin, Ruxolitinib, Lopinavir, Ritonavir, and Azithromycin) as presented in **Table 2**. The docking view of compounds **19** and **35** in the binding site of the protein is displayed in **Figures 3** and **4**, respectively. The main interactions between the ligands and proteins are seen to be conventional hydrogen bonding, Van der Waals, pi-cation, pi-anion, pi-sigma, and pi-alkyl bonds. Compound **19** (*N*-(benzo[*d*][1,3] dioxol-5-ylmethyl)-4-(benzofuro[3,2-*d*]pyrimidin -4- 4yl) piperazine-1-carbothioamide) binds to the protein site through four conventional H-bond formations, between HN of the ligand, and the O of Lys116, Tyr150, His141, and Tyr253, with bond distances of 6.22 Å, 4.61 Å, 5.41 Å, and 4.58 Å, respectively. The complex also formed a carbon-hydrogen bond between C of the ligand and the O of Phe147 with bond distances of 4.55 Å. Van der Waals' interactions with the protein are Leu120 and Phe117. As depicted in **Figure**

3A, there is also hydrophobic interaction between the ligand and the Ile252 (pi-sigma), Tyr150, Met153, and Cys118 (alkyl, pi-alkyl, and pi-pi T-shaped) respectively. The 3D docking view of compound **19** is presented in **Figure 3B**.

Figure 4(**A** and **B**) shows the docking view of compound **35** and the protein. The convectional hydrogen bond, carbon-hydrogen bond, and hydrophobic interaction (pi-sigma, alkyl, and pi-alkyl), respectively, were found to be the main collaboration between the ligand and the receptor (protein). Compound **35** has a lowing binding affinity score of 8.00 kcal/mol, were found to have four conventional H-bond with Ser121 (H---O), Leu550 (O----H), Asn240 (HN----O), Arg551 (H----O), Glu170 (O----HN), Lys167 (O----H), Arg118 (O-----C), and Ile241 (O----C). The hydrogen bonding distances are 3.18 Å, 4.03 Å, 4.91 Å, and 6.25 Å, respectively.

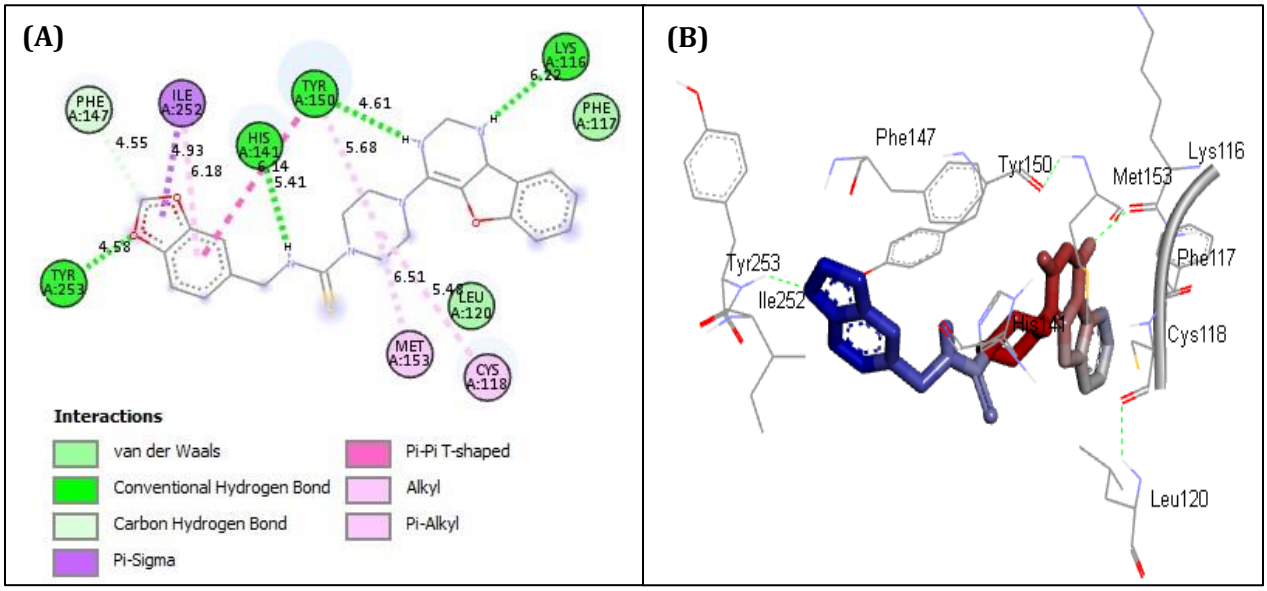

Figure 3. Docked interaction of compound **19** in the binding site of receptor PDB code: 5VK2 (A and B)

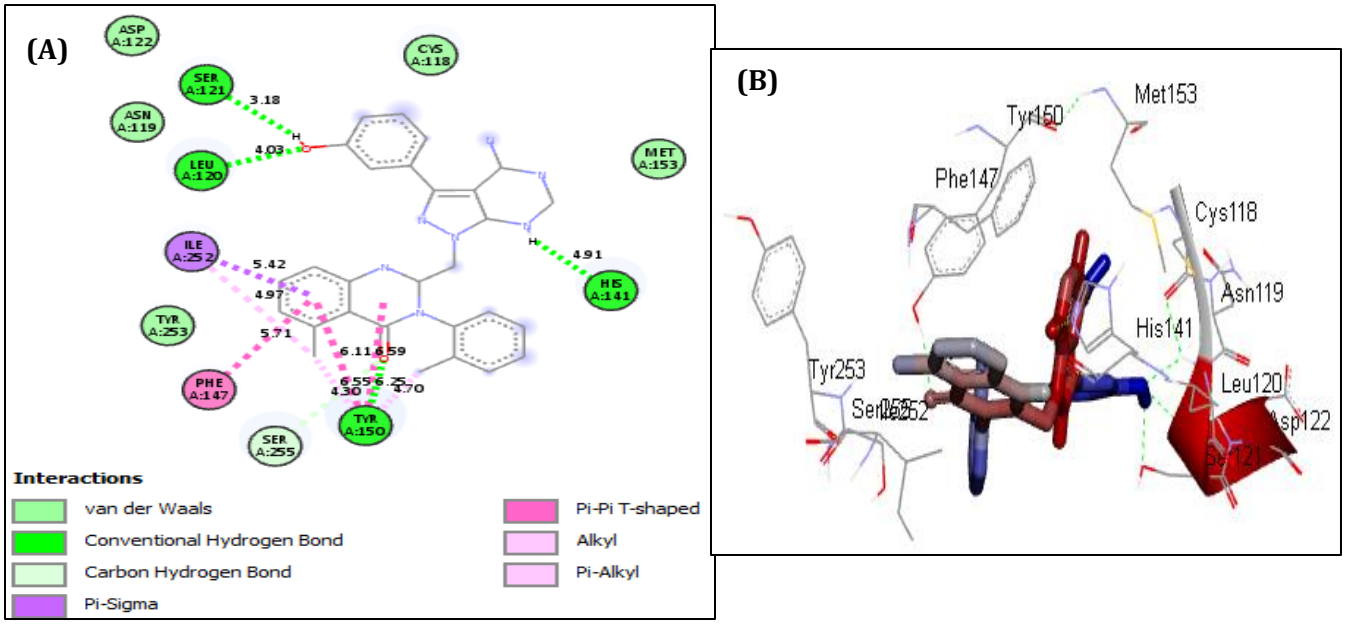

Figure 4. Docking interaction of compound **35** in the binding site of receptor PDB code: 5VK2 (A and B)

One carbon-hydrogen bond with Ser225 is with a bond distance of 4.30 Å. The complex also formed five Van der Waals' interactions with Asn119, Asp122, Cys118, Met153, and Tyr253, three (3) hydrophobic interactions with Ile252 pi-sigma bond, Tyr150, Phe147, and Ile252 (alkyl, pi-alkyl, and pi-pi T-shaped interactions), respectively.

Molecular Dynamics Simulations

The MD simulations of the protein-ligand complex demonstrate the complex stability and also allow extra information about the binding mode of compound **19** and compound **35**. The root means square deviation (RMSD), Root mean square fluctuation (RMSF), and solvent accessible surface area (SASA) plot during the MD simulations at 1000 trajectory are shown in **Figures 5A-5C**, respectively.

For this MD simulation, a 10 ns the protein-ligand complex architectures of glycoprotein complexes bound to compounds **19** and **35** were subjected to unconstrained simulation. Despite the initial structural arrangements of the docked complex, the average RMSD of the trajectories for bound protein backbone atoms was relatively stable. The stable RMSD values of the atoms for docked compounds **19** and **35** with the receptor are shown in **Figure 5A**. After 2 ns and 4 ns, the receptors arrive at equilibration and sway around a normal worth, according to the RMSD analysis. The average RMSDs for compounds **19** and **35** complexes from 1 ns to 10 ns were 3.19 Å and 2.90 Å, respectively, indicating structural stability and less flexibility. The relative stability of both compounds bound to the Lassa fever receptor was demonstrated by these RMSD results throughout the simulation. This result suggests that both compounds undergo a negligible primary conformational change during the 10 ns MD simulations.

The time-averaged RMSF value of the complexes after binding with the GP complex of the LASV receptor was measured over the last 10 ns of the simulation trajectory data to assess local protein quality. To characterize the mobility of individual residues, the flexibility of each complex was calculated by estimating the RMSF of compound **19** and compound **35** generated during the simulation, as shown in **Figure 5B**. The structure of all complexes does not change significantly during the simulation, as demonstrated in the **Figure**. Even though complex 35 has a higher fluctuation than complex 19, all complex graphs have a similar shape. The highest peaks in the RMSF plot indicate that those residues fluctuate a lot. The variations of residues in chemical binding pockets suggest that interactions of the selected compounds at the receptor's active site may improve the stiffness of the amino acids in the active site. This indicates that all complexes keep stable along with the simulation.

Based on the protein's solvent accessibility, the SASA plots show the rate of conformational changes. The protein-ligand complexes of compounds **19** and **35**, the average values of the complexes are 11.8404718 $Å^2$ and 10.23441899 $Å^2$, respectively (**Figure 5C**). The simulated systems were watched to see how the receptor's overall shape changed throughout the simulation. The SASA plot demonstrated that the SASA of complex-19 (3–6 ns) grew gradually until the equilibration period, and then plateaued at approximately 9 ns. This shows that the ligand was strongly bound in the binding pocket after equilibration, rendering the pocket inaccessible to bulk solvent. Comparing the configuration of the complex after stimulation with the docking confirmation, as shown in **Figures 3** and **4**, compound **19** assumes a similar docking location with the protein but moves richer in the protein's binding pocket, increasing the binding affinity substantially. After the simulation, the residues that bind to compound **19** established a typical hydrogen bond with Tyr253 at a distance of 5.69 nm (or Å), as illustrated in **Figure 6A**. Furthermore, at distances of 4.78 and 5.66, formed a series of carbon-hydrogen bonds with Ile144 and Leu142. Tyr150 (pi-pi stacked) and Leu142 (pi-alkyl) created two hydrophobic contacts with the ligand. Pi stacking is a non-covalent interaction between aromatic rings that plays a key function in various biological and chemical processes [46]. The protein also formed a series of Van der Waal's interactions with

Leu120, Cys118, Glu151, Ser255, Phe147, Asn146, Ile252, and Asp251 respectively. Ser121, Leu120, Tyr150, and His141 were identified to be involved in the creation of hydrogen bonds with the binding site area of LASV's glycoprotein during the docking simulation. Even though the key residues Ser121 and Cys118 helped form hydrogen bonds with the target protein at the end of the simulation, they further improved the protein-ligand complex's stability, as illustrated in **Figure 6B**.

We had a comprehensive grasp of the structure-activity relationship and binding modalities of the ligand for inhibitors of the glycoprotein (GPC) of LASV based on the results of CoMFA-FFD, CoMFA-UVEPLS, molecular docking, and MD simulations. The docking results validated the 3D-QSAR findings, which demonstrated the effect of each steric and electrostatic interaction on bioactivity. Molecular docking and MD simulations identified some critical interactions between the protein and the ligands at the same time. The MD simulations further explained hydrogen bond, steric "Van der Waal's interactions", and hydrophobic interactions on the ligands. The presence of constant hydrogen bonding and hydrophobic interactions between the protein-hit compounds **19** and **35** complexes caused the strongest interactions. These computer-based drug design or *in silico* studies would give helpful data and a useful asset for our next plan and streamlining of new practical glycoprotein complex of LASV inhibitors.

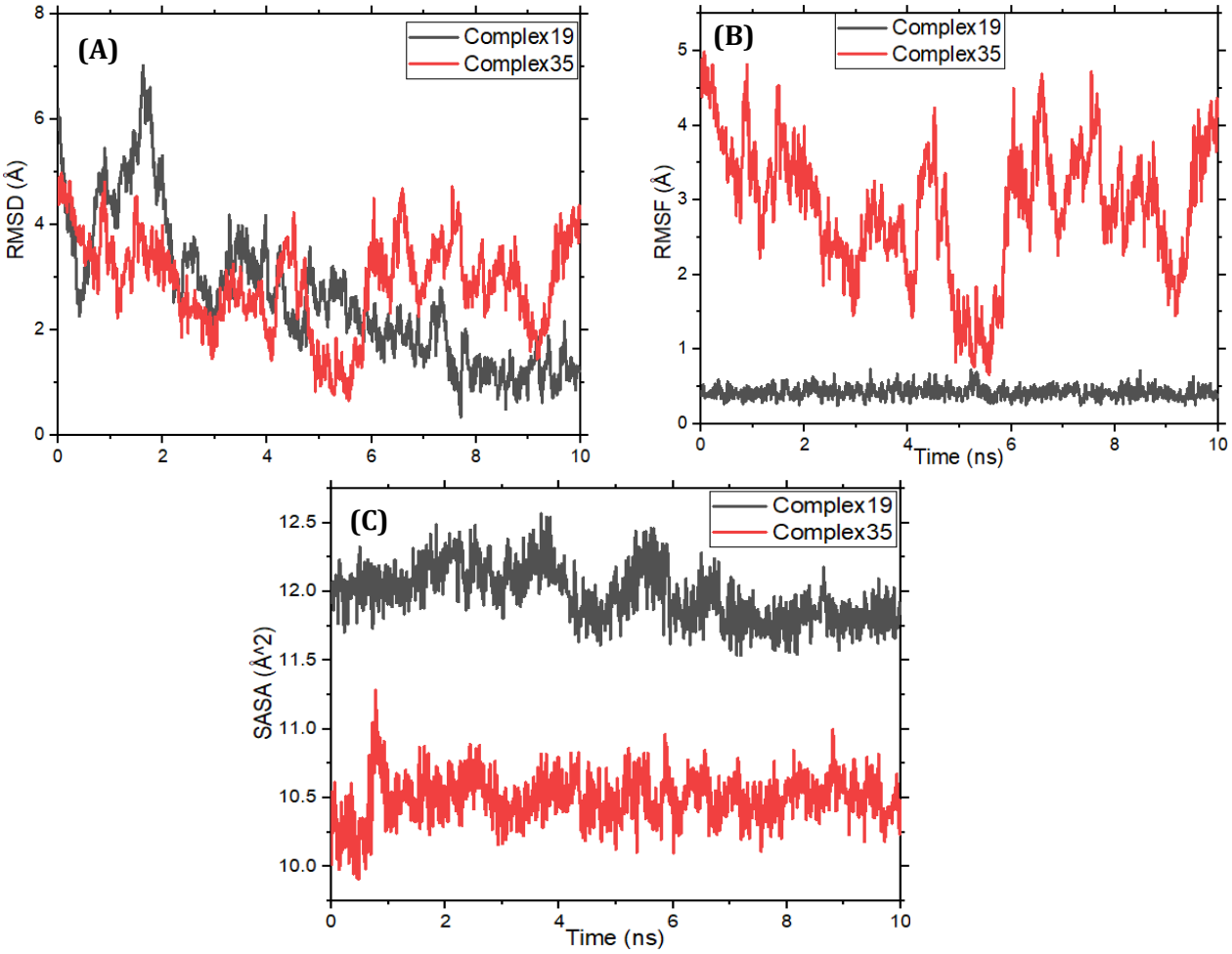

Figure 5. MDS study of glycoprotein (PDB ID: 5vk2) concerning (A) RMSD, (B) RMSF, and (C) SASA

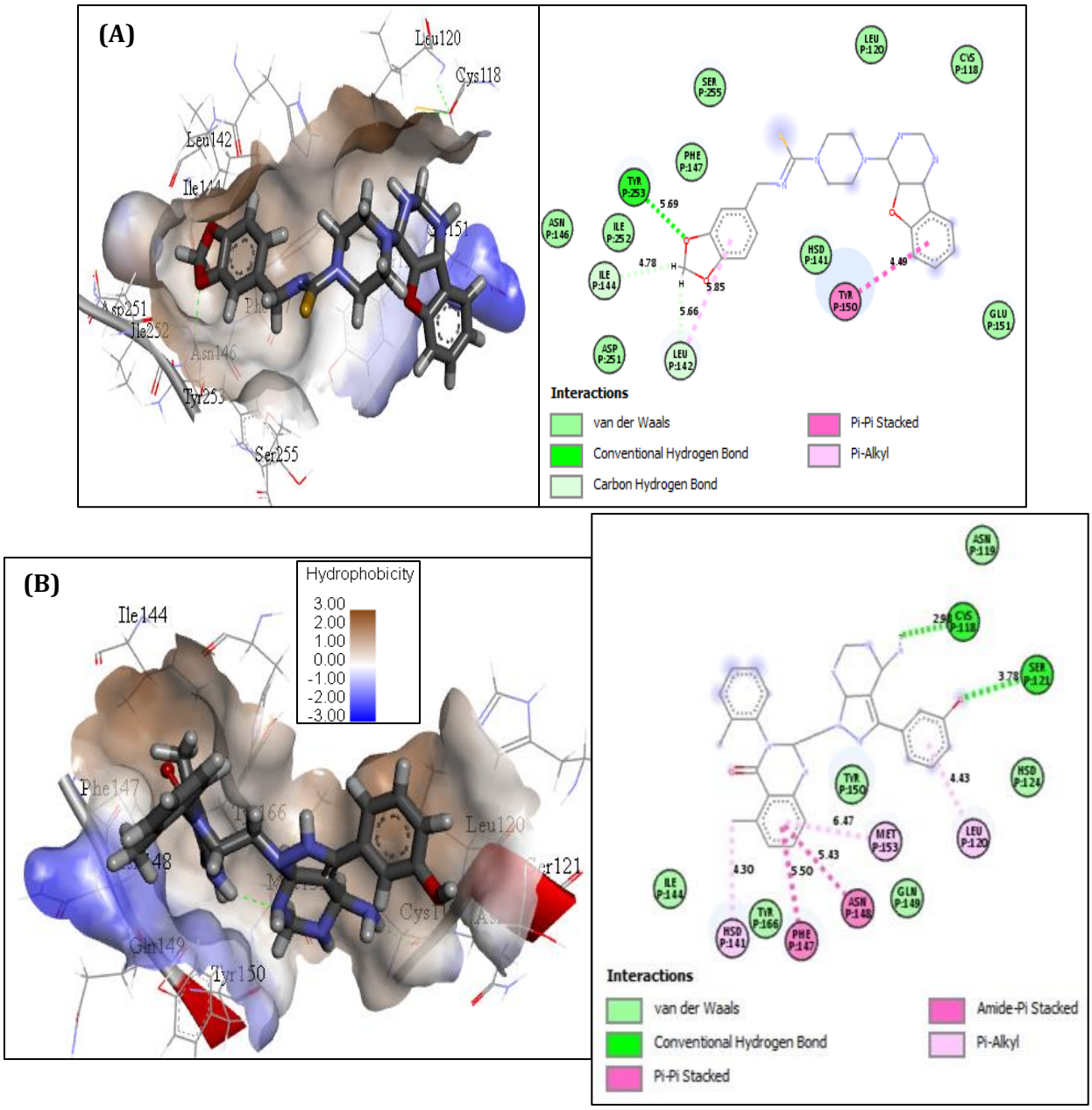

Figure 6. Molecular dynamics interactions of (A) compound **19** and (B) compound **35** with simulated protein structure

The structural properties of a protein may be influenced by its binding of a ligand, and SASA may change as a result. A higher SASA score denotes an increasing protein structure. The SASA value ought to vary just slightly throughout the simulation. Surface racing v5 was used to compute the solvent-accessible surface area (SASA) and other metrics in **Table 3** for both compounds [47]. The non-polar free energy can be calculated using the formula: $\triangle G_{SA}$ = γ × SASA + β [48], where γ = surface tension proportionality constant and β = the free energy of nonpolar solvation for a point solute. The values of the constants γ and β were 0.00542 kcalÅ^2 and 0.92 kcal/mol, respectively. The radius of the probe sphere used to calculate SASA was set to 1.4 Å.

The SASA value of compound **35** complex was lower than that of compound **19**. The total

average SASA value implies that compound **19** complexes may cause protein expansion, increasing the protein's solvent-accessible surface (**Table 3**). The electrostatic, Van der Waals and the non-polar energies of compounds **19** and **35** with glycoprotein (GPC) of LASV were presented in **Table 4**. The Van der Waals energy contributed significantly more to the binding energy than other energies, implying that Van der Waals energy interaction was important in the complex system. The internal energy was unfavorable for ligand binding, as indicated by the positive values in the case of complex **19**. This finding is consistent with the results of 3D-QSAR (CoMFA), docking, and MD simulations, which revealed that compound **35** has more interactions with the hydrophobic binding site.

Table 3. The solvent accessible surface area of the simulated complexes

The surface area of complex 19	The surface area of complex 35
Number of non-HOH, non-H atoms=1663	Number of non-HOH, non-H atoms=1016
Probe radius=1.40	Probe radius=1.40
TOTAL ASA=11719.58	TOTAL ASA=9930.23
TOTAL MSA=10265.85	TOTAL MSA=8295.32
Polar ASA=6586.11 Non-polar ASA=5133.47	Polar ASA=5076.53 Non-polar ASA=4853.70
Polar MSA=4700.38 Non-polar MSA=5565.48	Polar MSA=3578.53 Non-polar MSA=4716.78
Total backbone ASA=1962.55	Total backbone ASA=1613.86
Total backbone MSA=2543.22	Total backbone MSA=2072.09
Polar backbone ASA=1345.28	Polar backbone ASA=1148.13
Non-polar backbone ASA=617.27	Non-polar backbone ASA=465.74
Polar backbone MSA=1552.59	Polar backbone MSA=1317.12
Non-polar backbone MSA=990.63	Non-polar backbone MSA=754.98
Polar side chain ASA=5240.82	Polar side chain ASA=3928.40
Non-polar side chain ASA=4516.20	Non-polar side chain ASA=4387.97
Polar side chain MSA=3147.78	Polar side chain MSA=2261.42
Non-polar side chain MSA=4574.85	Non-polar side chain MSA=3961.80
+charge ASA=551.00 -charge ASA=839.28	+charge ASA=280.93 -charge ASA=551.69
+charge MSA=280.54 -charge MSA=376.18	+charge MSA=129.17 -charge MSA=243.64

MSA: Molecular Surface Area and ASA: Accessible Surface Area

Table 4. The computed free binding energies of the simulated compounds (kcal/mol)

Parameters	**Complex 19**			**Complex 35**		
	Complex	**Protein**	**Ligand**	**Complex**	**Protein**	**Ligand**
BOND	269.5412	264.459	6.6014	106.9596	96.7997	11.9063
ANGLE	562.1115	545.4876	18.1604	315.3269	285.0179	30.3831
DIHED	1,719.5106	1,654.8131	62.0238	1,101.9559	1,013.8331	89.7938
IMPRP	32.9232	32.1377	0.0115	15.3392	15.4766	0.0064
ELECT	-3,361.1568	-3,391.9027	33.9501	-1,656.3265	-1,379.6462	-266.1233
VDW	-700.7306	-690.0145	21.3692	-273.1361	-290.029	39.2074
ΔE(internal)			0.392		-3.6354	
ΔE(electrostatic) + deltaG(sol)			-3.2041		-10.5569	
ΔE(VDW)			-32.0852		-22.3145	
ΔG binding	-34.8974 +/- 0.4987 (kcal/mol)			-36.5068 +/- 0.8256 (kcal/mol)		

The calculated binding free energies ($\Delta G\ binding$) of complex **19** and complex **35** from the last 100 frames were -34.8974 +/- 0.4987 (kcal/mol) and -36.5068 +/- 0.8256 (kcal/mol), respectively (**Table 4**). The outcome demonstrates that the compounds remained in bound form for the simulation. When it comes to binding energy values, the binding energy value with the lowest negative value is the most potent [44]. Because more free energy is released as a result of this binding, the receptor and ligand make more contacts. As a result, unlike ligands with lower negative values, the intended target is more accessible. By comparing the ligands' binding energies (complex **19** and complex **35**), we may interpret the lowest experimental Fit LogAC50 value for compound **19** (-5.0529) compared to the experimental Fit LogAC50 of compound **35** (-4.4141) using the receptor produced by the molecular docking procedure. Therefore, compound **19** and compound **35** have the lowest binding affinity (-8 kcal/mol) compared to the reference drugs. As a result, compound 19's low Fit LogAC50 value reflects the molecule's high therapeutic activity. We should also mention that the binding affinity values of compound **14** are quite high (Fit_LogAC50 value: -7.0141) (binding affinity: -7.6 kcal/mol) and compound **17** (-7.9 kcal/mol) (Fit_LogAC50 value: -7.7641) were better than the binding affinity of the reference compounds (**Table 2**). Compounds **33**, **36**, and **41** with low Fit_LogAC$_{50}$ values of -4.6641, -7.1141, and -5.0641, respectively have the same binding affinity value as the reference drug (Azithromycin) (**Table 2**). The binding score compound (**19** and **35**), confirms that these compounds have higher biological activity in blocking the protein's enzymatic activity when compared to reference molecules.

We hypothesized that compound **19** would be the best in terms of calculating binding free energy for glycoproteins (GPC) and could exhibit higher potency than the references compounds, while compound **35** may have the potential to become specific glycoprotein (GPC) inhibitors based on the lines of evidence regarding delta G binding of surrounding atoms and SASA. These two selected hit-lead drugs discovered in this study could be interesting candidates for further GPC-targeting medicinal research and development.

Table 5. Contact frequency (%) analysis of 5VK2-19 and 5VK2-35 simulated complex

Find interactions:	**Complex-19**	**Find interactions**	**Complex-35**
Residue	Fraction	Residue	Fraction
PROA-CYS-118	47.35%	PROA-CYS-118	69.80%
PROA-LEU-120	24.78%	PROA-ASN-119	0.50%
PROA-HSD-141	99.56%	PROA-LEU-120	96.20%
PROA-LEU-142	100.00%	PROA-SER-121	65.20%
PROA-SER-143	10.62%	PROA-HSD-124	63.30%
PROA-ILE-144	99.56%	PROA-SER-138	0.50%
PROA-ASN-146	2.65%	PROA-HSD-141	99.70%
PROA-PHE-147	92.92%	PROA-LEU-142	61.30%
PROA-TYR-150	97.35%	PROA-ILE-144	5.10%
PROA-GLU-151	11.95%	PROA-PHE-147	98.20%
PROA-ASP-251	67.70%	PROA-ASN-148	75.90%
PROA-ILE-252	98.23%	PROA-GLN-149	59.10%
PROA-TYR-253	100.00%	PROA-TYR-150	95.60%
PROA-SER-255	15.93%	PROA-MET-153	68.70%
		PROA-TYR-166	2.10%

To further analyze the binding between 5VK2 and the compounds during the 10 ns MD simulation, the contactFreq.tcl module in VMD (cut-off of 4) was used. The proportion of the two ligands that were put to the test, compounds **19** and **35** that had contact frequency (CF) with the binding residues of 5VK2 was reported. The results indicate that some of the residues are involved in ongoing interactions with the compounds (**Table 5**).
The following amino acid residues showed higher CF values in the simulation study: HSD141, LEU142, ILE144, PHE147, TYR150, ASP251, ILE252, and TYR253 for complex **19**, and for complex **35**, the CF values with the greatest percentage scores are CYS118, LEU120, SER121, HSD124, LEU142, PHE147, ASN148, GLN149, TYR150, and MET153, respectively. The most common amino acids in both complexes are CYS118, LEU120, LEU142, ILE144, PHE147, and TYR150, as presented in **Table 5**.

Conclusion

This study reviewed the importance of CoMFA-FFD, CoMFA-UVEPLS, molecular docking, and MD simulations on drug discovery and design for inhibitors of the glycoprotein (GPC) of Lassa (LASV) Arenavirus. Our present studies have established that the structural features and binding mechanism of compounds **19** and **35** through Molecular Interaction Fields (MIFs) studies are quite reliable and significant. The CoMFA-FFD and CoMFA-UVEPLS studies indicate that the steric and electrostatic interaction plays an important role in determining the potency of the compounds. Docking on the same simulated A-chain of protein reveals that the ligand is bonded to conventional hydrogen bonds, carbon-hydrogen bonds, and hydrophobic interaction. Moreover, the ligand-protein complex was used in MD modeling to realize the conformation changes of the complex. The root mean square deviation (RMSD), root mean square fluctuation (RMSF), and solvent accessible surface area (SASA) plots demonstrated that the complex was stable, with the ligand-protein complex's shape changing minimally from the docking conformation. From these studies, we have added valuable information into the factors governing the potency of the inhibitors for the glycoprotein (GPC), of LASV.

Orcids

Emmanuel Israel Edache
https://orcid.org/0000-0002-5485-0583

Hadiza Adamu Dawi
https://orcid.org/0000-0002-8294-4173

Fabian Audu Ugbe
https://orcid.org/0000-0001-7052-4959

Acknowledgements

The authors gratefully acknowledged the technical effort of Dr. A.S. Ndaghiya, Department of Pure and Applied Chemistry, Faculty of Science, University of Maiduguri, P.M.B. 1069, Maiduguri, Borno State, Nigeria.

References

[1]. World Health Organization (WHO), Lassa Fever-Nigeria, **2020**. [Google Scholar], [Publisher]

[2]. L.N. Yamani, Y. Yano, T. Utsumi, W. Wasityastuti, H.T. Rinonce, D.I. Widasari, M.I. Lusida, Y. Hayashi, *Jpn. J. Infect. Dis.,* **2017**, *70*, 647-655. [Crossref], [Google Scholar], [Publisher]

[3]. S.K. Verma, S. Yadav, A. Singh, A. Kumar, *J. Drug Dev. Res.*, **2015**, *2*, 1008. [Crossref], [Publisher]

[4]. O. Ogbu, E. Ajuluchukwu, C.J. Uneke, *J. Vector Borne Dis.,* **2007**, *44***,** 1-11. [Crossref], [Google Scholar], [Publisher]

[5]. M. Hirschenberger, V. Hunszinger, K.M.J. Sparrer, *Cells*, 2021, *10*, 2134. [Crossref], [Google Scholar], [Publisher]

[6]. I.S. Usuwa, C.O. Akpa, C.D. Umeokonkwo, *BMC Public Health*, **2020**, *20,* 217. [Crossref], [Google Scholar], [Publisher]

[7]. E. Tambo, O.T. Adetunde, O.A. Olalubi, *Infec. Dis. Poverty*, **2018,** *7*, 74-80. [Google Scholar], [Publisher]

[8]. I.G. Madu, M. Files, D.N. Gharaibeh, A.L. Moore, K-H. Jung, B.B. Gowen *et al., PLoS Pathog*., **2018**, *14*, e1007439. [Crossref], [Google Scholar], [Publisher]

[9]. D. Kühnert, R. Kouyos, G. Shirreff, J. Pečerska, A.U. Scherrer, J. Böni, S. Yerly, T. Klimkait, V. Aubert, H.F. Günthard, *PLoS Pathog.,* **2018,** *14*, e1006895. [Crossref], [Google Scholar], [Publisher]

[10]. P. Wang, Y. Liu, G. Zhang, S. Wang, J. Guo, J. Cao, X. Jia, L. Zhang, G. Xiao, W. Wang, *J. Virol.,* **2018**, *92*, 00954-18. [Crossref], [Google Scholar], [Publisher]

[11]. B.M. Warner, D. Safronetz, D.R. Stein, *Drug Des. Devel. Ther.,* **2018**, *12***,** 2519-2527. [Google Scholar], [Publisher]

[12]. K.M. Hastie, M.A. Zandonatti, L.M. Kleinfelter, M.L. Heinrich, M.M. Rowland, K. Chandran, L.M. Branco, J.E. Robinson, R.F. Garry, E.O. Saphire, *Science*, **2017**, *356*, 923-928. [Crossref], [Google Scholar], [Publisher]

[13]. F. Lennartz, T. Hoenen, M. Lehmann, A. Groseth, W. Garten, *Arch Virol.,* **2013**, *158***,** 1895-1905. [Crossref], [Google Scholar], [Publisher]

[14]. K.M. Hastie, T. Liu, S. Li, L.B. King, N. Ngo, M.A. Zandonatti *et al., Proc. Natl. Acad. Sci.,* **2011**, *108,* 19365–19370. [Crossref], [Google Scholar], [Publisher]

[15]. S. Shafiu, E.I. Edache, U. Sani, M. Abatyough, *J. Pharm. Med. Res.,* **2017**, *3*, 78-80. [Crossref], [Google Scholar], [Publisher]

[16]. E.I. Edache, A. Uzairu, P.A. Mamza, G.A. Shallangwa, *Chem. Rev. Lett.,* **2021**, *4*, 130-144. [Crossref], [Google Scholar], [Publisher]

[17]. F.A. Ugbe, G.A. Shallangwa, A. Uzairu, I. Abdulkadir, *In Silico Pharmacol.*, **2022**, *10*, 8. [Crossref], [Google Scholar], [Publisher]

[18]. D. Madsen, C. Azevedo, I. Micco, I., L.K. Petersen, N.J.V. Hansen, *Prog. Med. Chem.,* **2020**, *59*, 181-249. [Crossref], [Google Scholar], [Publisher]

[19]. E.I. Edache, A. Uzairu, P.A. Mamza, G.A. Shallangwa, *J. Pharm. Sci.,* **2020**, *4***,** 21-36. [Crossref], [Google Scholar], [Publisher]

[20]. J. Mukherjee, R. Sharma, P. Dutta, B. Bhunia, *Biotechnol. Genet. Eng. Rev.,* **2023**, 1. [Crossref], [Google Scholar], [Publisher]

[21]. F.A. Ugbe, G.A. Shallangwa, A. Uzairu, I. Abdulkadir, *Chem. Data Collect.,* **2021**, *36,* 100783. [Crossref], [Google Scholar], [Publisher]

[22]. E.I. Edache, A. Uzairu, P.A. Mamza, G.A. Shallangwa, *J. Drug Design Discov. Res.*, **2020**, *1*, 36-52. [Crossref], [Google Scholar], [Publisher]

[23]. E.I. Edache, A. Uzairu, P.A. Mamza, G.A. Shallangwa, *Future J. Pharm. Sci.,* **2021**, *7*, 220. [Crossref], [Google Scholar], [Publisher]

[24]. A. Speck-Planche, V. Valeria. V.V. Kleandrova, T. Marcus, M.T. Scotti, M.N.D.S. Cordeiro, *Curr. Bioinform.,* **2013**, *8***,** 452-464. [Google Scholar], [Publisher]

[25]. S. Ahmad, H. W. abbasi, S. Shahid, S. Gul, S.W. Abbasi, *J. Biomol. Struct. Dyn.,* **202**1, *39*, 4225-4233. [Crossref], [Google Scholar], [Publisher]

[26]. A. Vaidya, A.K. Jain, P.B.R. Kumar, G.N. Sastry, S.K. Kashaw, R.K. Agrawal, *Arab. J. Chem.,* **2017,** *10*, S3936-S3946. [Crossref], [Google Scholar], [Publisher]

[27]. National Center for Biotechnology Information. PubChem Bioassay Record for AID 1347082, Source: National Center for Advancing Translational Sciences (NCATS), **2022**. [Publisher]

[28]. Wavefunction. Inc. Spartan'14, version 1.1.4, Irvine, California, USA. **2014**. [Publisher]

[29]. E.I. Edache, A. Uzairu, S.E. Abechi, *J. Comput. Aided Mol. Des.,* **2015**, *5*, 135-149. [Crossref], [Google Scholar], [Publisher]

[30]. K. Roy, I. Mitra, *Comb. Chem. High Throughput Screen.,* **2011**, *14*, 450-474. [Crossref], [Google Scholar], [Publisher]

[31]. M.A.K. Liton, A.C. Bhowmick, M.A. Ali, *Univers. J. Chem.,* **2013**, *1,* 71-76. [Crossref], [Google Scholar], [Publisher]

[32]. P. Tosco, T. Balle, F. Shiri, *J. Comput. Aided Mol. Des*., **2011**, *25*, 777-783. [Crossref], [Google Scholar], [Publisher]

[33]. E.I. Edache, A. Uzairu, P.A. Mamza, G.A. Shallangwa, *Sci. Afr.,* **2022**, *15*, e01088. [Crossref], [Google Scholar], [Publisher]

[34]. P. Tosco, T. Balle, *J. Mol. Model.,* **2011**, *17*, 201-208. [Crossref], [Google Scholar], [Publisher]

[35]. E.I. Edache, A. Uzairu, P.A. Mamza, G.A. Shallangwa, *J. Genet. Eng. Biotechnol.,* **2022**, *20*, 88. [Crossref], [Google Scholar], [Publisher]

[36]. G.M. Morris, D.S. Goodsell, R.S. Halliday, R. Huey, W.E. Hart, R.K. Belew, A.J. Olson, *J. Comput. Aided Mol. Des.,* **1998**, *19*, 1639-1662. [Crossref], [Google Scholar], [Publisher]

[37]. O. Trott, A.J. Olson, *J. Comput. Chem.,* **2010**, *31***,** 455-461. [Crossref], [Google Scholar], [Publisher]

[38]. M. Abbasi, H. Sadeghi-Aliabadi, F. Hassanzadeh, M. Amanlou, *J. Mol. Graph. Model.,* **2015**, *61*, 186-195. [Crossref], [Google Scholar], [Publisher]

[39]. J.C. Phillips, R. Braun, W. Wang, J. Gumbart, E. Tajkhorshid, E. Villa, C. Chipot, R.D. Skeel, L. Kale, K.S. Scalable, *J. Comput. Chem.,* **2005**, *26*, 1781-1802. [Crossref], [Google Scholar], [Publisher]

[40]. P.L. Barclay, D.Z. Zhang, *J. Comput. Phys.,* **2021,** *435*, 110238. [Crossref], [Google Scholar], [Publisher]

[41]. W. Humphrey, A. Dalke, K. Schulten, X VMD: visual molecular dynamics, *J. Mol. Graph.,* **1996**, *14***,** 33-38. [Crossref], [Google Scholar], [Publisher]

[42]. Q. Bai, S. Tan, T. Xu, H. Liu, J. Huang, X. Yao, *Brief. Bioinformatics,* **2021**, *22*, bbaa161. [Crossref], [Google Scholar], [Publisher]

[43]. F.A. Ugbe, G.A. Shallangwa, A. Uzairu, I. Abdulkadir, *In Silico Pharmacol.,* **2022**, *10***,** 21. [Crossref], [Google Scholar], [Publisher]

[44]. E.I. Edache, A. Uzairu, P.A. Mamza, G.A. Shallangwa, M. Azam, K. Min, *J. Mol. Struct.,* **2023**, *1289*, 135913. [Crossref], [Google Scholar], [Publisher]

[45]. E.I. Edache, A. Uzairu, P.A. Mamza, G.A. Shallangwa, *Turk. Comput. Theor. Chem.,* **2024**, *8***,** 10-39. [Crossref], [Google Scholar], [Publisher]

[46]. O. Haghighi, S. Davaeifar, H.S. Zahiri, H. Maleki, K.A. Noghabi, *Int. J. Pept. Res. Ther.,* **2020**, *26*, 783–793. [Crossref], [Google Scholar], [Publisher]

[47]. O.V. Tsodikov, M.T. Jr. Record, Y.V. Sergeev, *J. Comput. Chem.,* **2002,** *23*, 600-609. [Crossref], [Google Scholar], [Publisher]

[48]. V.K. Vishvakarma, N. Shukla, Reetu, K. Kumari, R. Patel, P. Singh, , *Heliyon*, **2019**, *5*, e02124. [Crossref], [Google Scholar], [Publisher]